

Symmetry enhanced first-order phase transition in a two-dimensional quantum magnet

Bowen Zhao, Phillip Weinberg, Anders W Sandvik. "Symmetry enhanced first-order phase transition in a two-dimensional quantum magnet."

<https://hdl.handle.net/2144/32889>

"Downloaded from OpenBU. Boston University's institutional repository."

Symmetry enhanced first-order phase transition in a two-dimensional quantum magnet

Bowen Zhao,¹ Phillip Weinberg,¹ and Anders W. Sandvik^{1,2,*}

¹*Department of Physics, Boston University, 590 Commonwealth Avenue, Boston, Massachusetts 02215, USA*

²*Beijing National Laboratory for Condensed Matter Physics and Institute of Physics, Chinese Academy of Sciences, Beijing 100190, China*
(Dated: May 3, 2018)

Theoretical descriptions of quantum phase transitions have indicated the existence of critical points with higher symmetries than those of the underlying Hamiltonian. Here we present an example of such an emergent symmetry at a first-order transition, where coexistence of two ordered phases takes the form of a higher rotational symmetry in the space of the two order parameters. Using quantum Monte Carlo simulations, we study a two-dimensional (2D) $S = 1/2$ quantum magnet hosting the antiferromagnetic (AFM) and plaquette-singlet solid (PSS) states recently detected in $\text{SrCu}_2(\text{BO}_3)_2$. We observe that the $O(3)$ symmetric AFM order and the Z_2 symmetric PSS order form an $O(4)$ vector at the transition. The control parameter (a coupling ratio) rotates the vector from the AFM sector to the PSS sector, with the length of the combined order parameter vector always remaining non-zero. This phenomenon should be observable in $\text{SrCu}_2(\text{BO}_3)_2$.

Introduction.—Theoretical studies of exotic quantum states of matter and the phase transitions between them can provide new perspectives on many-body physics and stimulate experimental investigations. A prominent example is the quantum phase transition between antiferromagnetic (AFM) and spontaneously dimerized valence-bond solid (VBS) states in two-dimensional (2D) spin $S = 1/2$ magnets [1, 2]. Here the theory of deconfined quantum critical points (DQCPs) suggests that the Landau-Ginzburg-Wilson (LGW) paradigm for phase transitions is inapplicable, as a consequence of quasi-particle fractionalization [3, 4]. Over the past decade, likely DQCPs have been identified in lattice models, using “designer hamiltonians” constructed for their amenability to large-scale quantum Monte Carlo (QMC) simulations of the AFM–VBS transition [5–16]. Recently, a potential experimental realization of this type of DQCP was reported in the quasi-2D Shastry-Sutherland (SS) compound $\text{SrCu}_2(\text{BO}_3)_2$ under pressure [17]. Though the SS model [18] is difficult to study numerically, due to its geometrical frustration (which causes sign problems in QMC simulations), a specific type of VBS—a two-fold degenerate plaquette-singlet solid (PSS) located between AFM and bond-singlet phases—was demonstrated convincingly by tensor-network calculations [19]. Zayed et al. [17] showed that a PSS also exists in $\text{SrCu}_2(\text{BO}_3)_2$ and suggested that the AFM–PSS transition may be a DQCP. The phase transition was not studied in the experiment, however, and it is not immediately clear if the two-fold degenerate PSS can support spinon deconfinement in the same way as a four-fold degenerate VBS. QMC studies of rectangular lattices with two-fold degenerate VBS states point to a first-order transition [13], as was also found in the SS model [19].

Here we study a sign-free model that mimics the SS compound, in the sense that it shares the same kinds of AFM and PSS ground states. The Hamiltonian, illustrated in Fig. 1 along with the SS model, is a new member in the “ J - Q ” family [5], with Heisenberg exchange J supplemented by four-spin interactions Q that weaken and eventually destroy the AFM order. Our QMC simulations demonstrate a first-order AFM–PSS transition with emergent $O(4)$ symmetry.

Non-LGW critical points with emergent higher symmetries

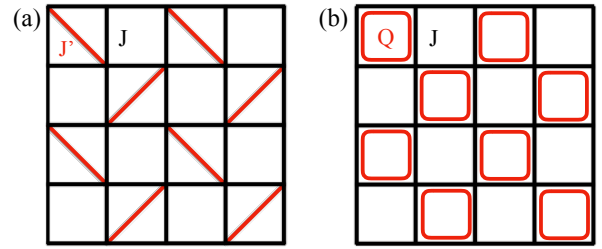


Figure 1. In the SS model (a), Heisenberg exchange J between nearest neighbor $S = 1/2$ spins compete with next-nearest neighbor couplings indicated by diagonal lines. In the CBJQ model (b) the J' interactions are replaced by the Q terms in Eq. (1).

have been extensively investigated during the past few years [20–30]. In the case discussed here, the order parameters exhibit clear discontinuities but conventional phase coexistence is not observed. We show that the AFM order is rotated by the control parameter into PSS order, and that the phase coexistence at the transition is in the form of an $O(4)$ symmetric vector order parameter arising out of the $O(3)$ (AFM) and Z_2 (PSS) order parameters. The transition is, thus, similar to that in a system tuned through a point with continuous symmetry G that separates ordered phases whose symmetries are subgroups of G . A well known case is the XXZ spin model tuned from the $O(2)$ phase through the $O(3)$ symmetric Heisenberg point into the Z_2 (Ising) phase. However, in our system the different components of the $O(4)$ vector are physically distinct, not just different components of a magnetic order parameter, and the symmetry is emergent instead of explicit.

Ground states.—Our Hamiltonian can be defined using single projection operators $P_{ij} = (1/4 - \mathbf{S}_i \cdot \mathbf{S}_j)$;

$$\mathcal{H} = -J \sum_{\langle ij \rangle} P_{ij} - Q \sum_{ijkl \in \square'} (P_{ij} P_{kl} + P_{ik} P_{jl}), \quad (1)$$

where all indicated site pairs are nearest neighbors on a periodic square lattice with $N = L^2$ sites and \square' denotes the 2×2 Q -plaquettes in Fig. 1(b). We define $g = J/Q$. For $g \rightarrow \infty$, this checker-board J - Q (CBJQ) model reduces to the usual

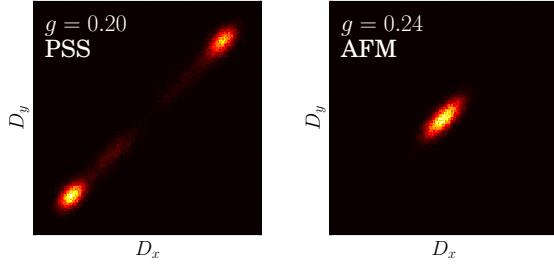


Figure 2. Dimer order distribution $P(D_x, D_y)$ in the ground state of the CBJQ model at $g = 0.20$ (in the PSS phase) and at $g = 0.24$ (in the AFM phase), from valence-bond QMC on $L = 96$ lattices.

AFM ordered (at temperature $T = 0$) Heisenberg model, and for $g \rightarrow 0$ we will demonstrate a two-fold degenerate PSS. The model does not have any phase corresponding the J' -bond singlet state of the SS model for large J'/J . However, for elucidating the nature of the AFM–PSS transition, we can invoke symmetries and universality to propose that the two models, as well as $\text{SrCu}_2(\text{BO}_3)_2$, contain the same physics.

We use two different QMC methods to study the CPJQ model: ground-state projection in the basis of valence bonds [31] and the stochastic series expansion (SSE) method [32]. Both techniques deliver exact results to within statistical errors. The projector method is very useful for studying spin-rotationally averaged quantities, while the SSE method is more efficient for finite-size scaling when the finite- L ground states do not have to be fully reached but $T \rightarrow 0$ as $L \rightarrow \infty$.

To demonstrate the PSS ground state for large g , we first study a conventional dimer order parameter

$$D_\mu = \frac{1}{N} \sum_{\mathbf{r}} (-1)^{r_\mu} \mathbf{S}(\mathbf{r}) \cdot \mathbf{S}(\mathbf{r} + \hat{\mu}), \quad \mu = x, y, \quad (2)$$

where the sum is over the lattice sites at $\mathbf{r} = (r_x, r_y)$. In a columnar symmetry-broken VBS $\langle D_x \rangle \neq 0, \langle D_y \rangle = 0$ for x -oriented bond order and the same with $x \leftrightarrow y$ for y oriented bonds. Since a singlet plaquette can be regarded as a resonance between horizontal and vertical bond pairs, a two-fold degenerate PSS should have $|\langle D_x \rangle| = |\langle D_y \rangle| \neq 0$ due to modulated singlet density on the plaquette rows and columns in Fig. 1. On a finite lattice the symmetry is not broken, and the system fluctuates between the two states. We use the projector method to generate the probability distribution $P(D_x, D_y)$. While strictly not a quantum mechanical observable, this distribution nevertheless properly reflects the fluctuations and symmetries of the system. Results on either side of the AFM–PSS transition (the location of which will be determined below) are shown in Fig. 2. We see the two-fold symmetry of a PSS, instead of the four-fold symmetry of the columnar VBS [9, 33] that also is compatible with the lattice.

If the Q terms are included on all plaquettes we arrive back to the original J - Q model, whose AFM–VBS transition ap-

pears to be continuous [16]. In accord with the DQCP theory, an emergent $U(1)$ symmetry of its microscopically Z_4 invariant VBS order parameter has been confirmed [5, 7, 33]. The proposed field theory description with spinons coupled to an $U(1)$ gauge field [3, 4] therefore seems viable. Unusual finite-size scaling behaviors not contained within the theory (but not contradicted by it) have also been observed [10, 15, 16] (and interpreted by some as a weak first-order transition [7, 8, 11]). An interesting proposal is that the $O(3)$ symmetry of the AFM and the emergent $U(1)$ symmetry of the VBS may combine into an $SO(5)$ symmetry exactly at the critical point [20, 34]. In a spin-planar J - Q model, it has instead been demonstrated that the $U(1)$ AFM order parameter and the emergent $U(1)$ VBS symmetry combine into an emergent $O(4)$ symmetry [26]. In yet another example, it was proposed that a system with $O(3)$ AFM order and Z_2 Kekule VBS state exhibits a DQCP with emergent $SO(4)$ symmetry [27]. The $O(3)$ and Z_2 symmetries apply also to the CBJQ model, and we therefore pay attention to a potential $O(4)$ or $SO(4)$ symmetry [35].

Finite-size scaling.—To analyze the AFM–PSS transition, we perform SSE calculations at $T = 1/L$. This way of taking the limit $T \rightarrow 0, L \rightarrow \infty$ is appropriate for a quantum phase transition with dynamic exponent equal to unity, as well as a for a first-order transition. We use order parameters defined solely with the S^z spin components,

$$m_z = \frac{1}{N} \sum_{\mathbf{r}} \phi(\mathbf{r}) S^z(\mathbf{r}), \quad m_p = \frac{2}{N} \sum_{\mathbf{q}} \theta(\mathbf{q}) \Pi^z(\mathbf{q}), \quad (3)$$

where the subscripts z (spin component) and p (plaquette) mark the AFM and PSS order parameters, respectively. In m_z , \mathbf{r} runs over all N lattice sites and $\phi(\mathbf{r}) = \pm 1$ is the staggered AFM sign. In m_p , we have defined an operator

$$\Pi^z(\mathbf{q}) = S^z(\mathbf{q}) S^z(\mathbf{q} + \hat{x}) S^z(\mathbf{q} + \hat{y}) S^z(\mathbf{q} + \hat{x} + \hat{y}), \quad (4)$$

for detecting plaquette modulation, and the index \mathbf{q} runs over the low-left corners of the Q plaquettes in Fig. 1. The signs $\theta(\mathbf{q}) = \pm 1$ correspond to even or odd plaquette rows.

We will primarily analyze the Binder cumulants,

$$U_z = \frac{5}{2} \left(1 - \frac{\langle m_z^4 \rangle}{3 \langle m_z^2 \rangle^2} \right), \quad U_p = \frac{3}{2} \left(1 - \frac{\langle m_p^4 \rangle}{3 \langle m_p^2 \rangle^2} \right), \quad (5)$$

where the coefficients have been chosen according to the relevant symmetries so that $U_z \rightarrow 1, U_p \rightarrow 0$ in the AFM phase while $U_z \rightarrow 0, U_p \rightarrow 1$ in the PSS. If there is a single transition, we can use the crossing point $g = g^*(L)$ at which $U_z(g, L) = U_p(g, L)$ to define a finite-size critical point $g^*(L)$. We can also take the more commonly used crossing points of curves for two different system sizes, L and bL (where we use $b = 2$), locating the g value where $U_z(g, L) = U_z(g, bL)$ or $U_p(g, L) = U_p(g, bL)$. The three definitions will differ for finite L but should flow to the same point g_c in the thermodynamic limit.

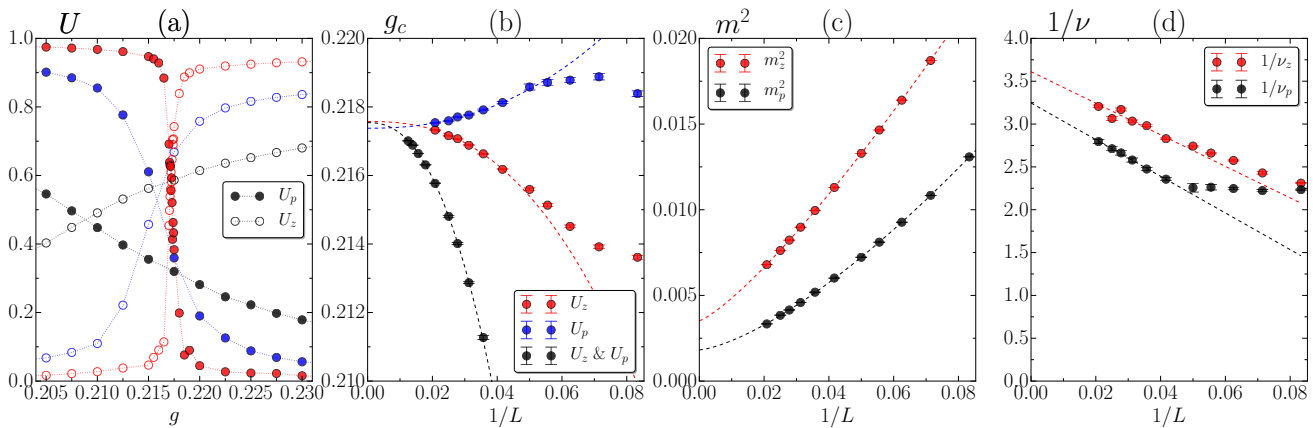


Figure 3. Finite-size scaling of CBJQ results from SSE simulations at $T = 1/L$. (a) Spin (open symbols) and plaquette (solid symbols) Binder cumulants versus g for $L = 24$ (black), 48 (blue) and 96 (red). Interpolations within these data sets (and results for other system sizes) underlie the analysis presented in the other panels. In (b) the crossing g -values of U_z and U_p are shown vs $1/L$ along with the $(L, 2L)$ same-quantity crossing points from U_z and U_p . The points approach the infinite-size transition point $g_c = 0.2175 \pm 0.0001$. The curves are fits including a single power-law correction $\propto L^{-\omega}$. In (c) the squared order parameters at the Binder $(L, 2L)$ cross points are graphed versus $1/L$ along with polynomial fits. The estimator of the correlation-length exponent, Eq. (6), is shown in (d) for both order parameters, along with line fits. In all fits, small system sizes were excluded until acceptable agreement with the functional forms were obtained.

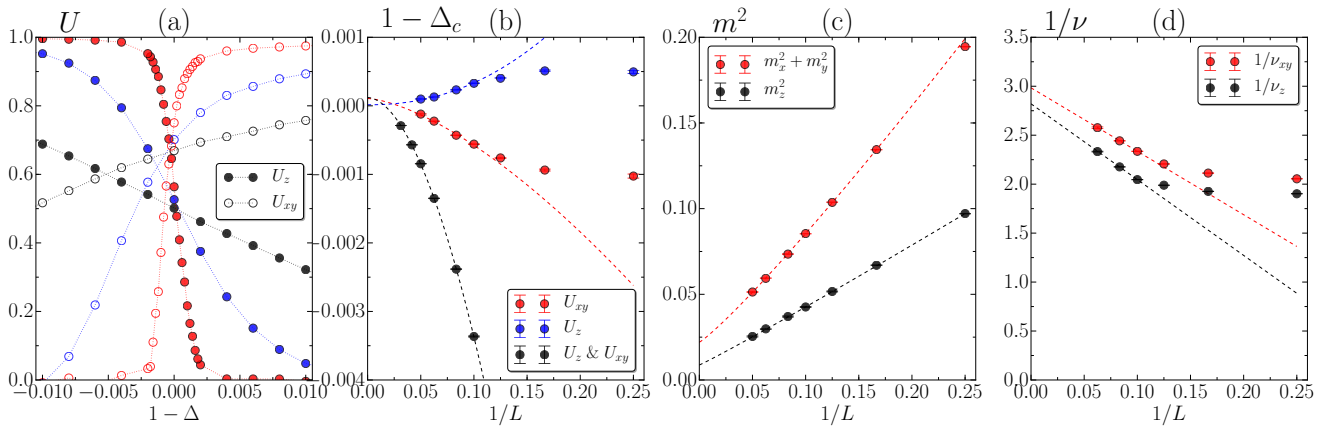


Figure 4. Results for the classical 3D Heisenberg model with anisotropy Δ graphed as in Fig. 3. Here $T^{-1} = 0.7 > T_c^{-1}$ for all values of Δ . The system sizes in (a) are $L = 8$ (black), 16 (blue) and 32 (red), with open and solid symbols used for U_{xy} and U_z , respectively. In the other panels the analysis is presented as in Fig. 3.

The slopes of the cumulants at g_c can be used to extract the correlation length exponents ν_z and ν_p , using two system sizes, L and bL [16, 36]:

$$\frac{1}{\nu_{zp}} = \frac{1}{\ln(b)} \ln \left[\frac{dU_{zp}(g, bL)/dg}{dU_{zp}(g, L)/dg} \right]_{g=g_c(L)}, \quad (6)$$

where $g_c(L)$ is the relevant (L, bL) cross point. The derivatives can be evaluated directly in the QMC simulations, and we interpolate to obtain the cross points and slopes from data on a dense g -grid in the neighborhood of g_c .

The analysis is presented and explained in Fig. 3. We find a single transition with $g_c = 0.2175 \pm 0.0001$ based on all three cross point estimators in Fig. 3(b). Most notably, in Fig. 3(c) the order parameters at their respective Binder crossing points do not vanish as $L \rightarrow \infty$. This coexistence of AFM and PSS

order is a decisive indicator of a first-order transition. Another first-order indicator is $1/\nu_z$ and $1/\nu_p$ growing to values larger than 3 with increasing L . At a classical first-order transition, $1/\nu \rightarrow d$, where d is the spatial dimensionality. Here, in 2+1 dimensions we might expect $1/\nu_{zp} \rightarrow 3$, but in Fig. 3(d) we see larger values, perhaps related to the Anderson-Goldstone rotor spectrum of the coexistence state. In any case, the large values do not support the already ruled-out continuous transition. Then one would normally also expect divergent negative peaks in the Binder cumulants [37, 38], which are not seen in Fig. 3(a) but are present at the first-order transition in a J - Q model with staggered Z_4 VBS [39].

The lack of negative Binder peak at the first-order transition leads us to consider alternative scenarios for coexisting order parameters. A well known case is a system with long-range

order driven through a point at which the Hamiltonian has a higher symmetry. As an example, we discuss a deformed 3D classical Heisenberg O(3) model in its ordered phase, with nearest neighbor interactions $H_{ij} = \sigma_i^x \sigma_j^x + \sigma_i^y \sigma_j^y + \Delta \sigma_i^z \sigma_j^z$ between unit vectors σ_i on a simple cubic lattice. We could also consider the 2D $S = 1/2$ AFM Heisenberg model at $T = 0$ with a similar deformation [40]. When $\Delta < 1$, the order parameter is U(1) symmetric in the xy plane, while for Ising anisotropy, $\Delta > 1$, the symmetry is Z_2 . At the O(3) point $\Delta = 1$, the elementary excitations of the quantum model change, as the Goldstone modes of the U(1) phase and O(3) point are gapped out continuously for $\Delta > 1$. In this sense we can consider the change in symmetry as a phase transition with both first-order and continuous characteristics.

We carry out classical Monte Carlo simulations at $T^{-1} = 0.7$, close to $T_c^{-1}(\Delta_c = 1) \approx 0.6930$, and analyze the xy and z magnetizations individually. As shown in Fig. 4, behaviors very similar to those in the CPJQ model are observed if we make an analogy between the xy magnetization and the AFM order parameter on the one hand and the Ising magnetization and the PSS order parameter on the other hand. The Binder cumulants and slopes are defined in ways analogous to Eqs. (5) and (6). Since T is barely below T_c , the coexistence values $\langle m_x^2 \rangle = \langle m_y^2 \rangle = \langle m_z^2 \rangle$ in Fig. 4(c) are small. In Fig. 4(d) we can also see that $1/\nu_{xy}$ approaches the expected first-order value 3, using a simple line fit, while a proper analysis of $1/\nu_z$ may require larger systems.

In most respects, we see that the O(3) order–order transition looks in finite-size scaling as a first-order transition, with the glaring exception of the lack of negative Binder peak. Indeed, with phase coexistence in the form of a higher symmetry, the arguments behind the negative peak [37, 38] do not apply.

Emergent O(4) symmetry.—The CBJQ model does not have any obvious point of enhanced symmetry, but the above results suggest that the system possesses an emergent symmetry at g_c . The most natural scenario is that the O(3) AFM and the Z_2 PSS combine to form O(4) symmetry [35]. To test this, we use the valence-bond projector QMC method and now define m_p with the rotationally invariant operator,

$$\begin{aligned} \Pi(\mathbf{q}) = & \mathbf{S}(\mathbf{q}) \cdot \mathbf{S}(\mathbf{q} + \hat{x}) + \mathbf{S}(\mathbf{q} + \hat{y}) \cdot \mathbf{S}(\mathbf{q} + \hat{y} + \hat{x}) \\ & + \mathbf{S}(\mathbf{q}) \cdot \mathbf{S}(\mathbf{q} + \hat{y}) + \mathbf{S}(\mathbf{q} + \hat{x}) \cdot \mathbf{S}(\mathbf{q} + \hat{x} + \hat{y}), \end{aligned} \quad (7)$$

in place of $\Pi^z(\mathbf{q})$ in Eq. (3). We investigate the probability distribution $P(m_z, m_p)$, where the z -component of the AFM order parameter is given as before by Eq. (3) and both m_z and m_p can be generated from a given transition graph [31]. In a state with both AFM and PSS order, the commutator $[m_z, m_p] \propto 1/N$, and we can treat m_z and m_p as c -numbers. For the putative O(4) symmetry to be manifest, we further normalize each m_z and m_p by factors involving $\langle m_z^2 \rangle$ and $\langle m_p^2 \rangle$, as explained in Supplemental Material [42].

For a point on an O(4) sphere of radius R , the projection onto two components results in a uniform distribution within a circle of radius R . However, in a finite system we also expect fluctuations of R , and we therefore compare our CBJQ results with a distribution obtained from an O(4) sphere with

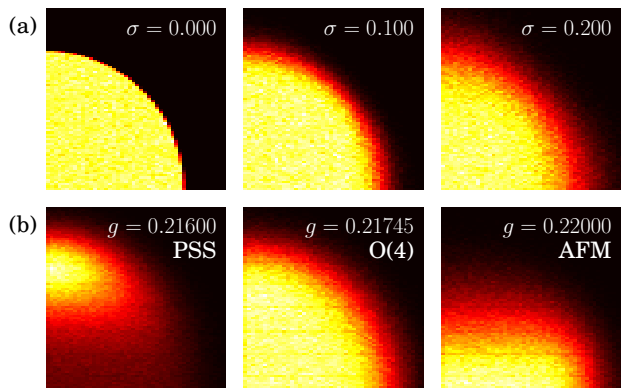


Figure 5. (a) One quadrant of the sampled [41] distribution of two components of an O(4) vector with Gaussian length fluctuations with mean $R = 1$ and standard deviation σ . (b) Projector QMC distribution $P(m_z, m_p)$ for the $L = 64$ CBJQ model at three coupling parameters g . The x axis represents the z component of the AFM order parameter (m_z), while the y -axis is the PSS order parameter (m_p) [42].

mean radius $R = 1$ and standard deviation σ . Examples are shown Fig. 5. At the transition, the CBJQ distribution is rotation symmetric with radial profile similar to that of the O(4) sampling with $\sigma = 0.2$. Inside the phases the distributions are shifted as expected—deep in the PSS we should eventually, for $L \rightarrow \infty$, obtain a point on the y -axis, and in the AFM state a line on the x -axis. Further tests of the emergent symmetry are presented in Supplemental Material [42].

Discussion.—We have found a first-order quantum phase transition at which coexisting AFM and PSS order parameters form an emergent O(4) vector. It is possible that the O(4) symmetry is not exact, but reflects the existence of a nearby fixed point (perhaps outside the model space) at which the higher symmetry is exact [20, 25, 28]. Then, away from this point, perturbations break the symmetry above some length scale ξ' larger than the correlation length ξ [25]. This scenario was discussed in the context of continuous and weakly first-order transitions. In the case of the CBJQ model, the observed discontinuities are rather large, however. From Fig. 3(c) and assuming O(4) symmetry, we have $m_s = \langle 4m_z^2 \rangle^{1/2} \approx 0.12$, almost 25% of the maximum (classical) staggered magnetization. Moreover, the first-order nature of the transition is apparent even on small lattices, e.g., the flow of $1/\nu_z$ in Fig. 3(d). Thus, we are well above the length scale ξ but the scenario of Ref. [25] would suggest that still $L \ll \xi' \sim \xi^{1+a}$, where the exponent a would have to be rather large in order to give the clear separation of length scales needed to account for the observed O(4) behavior. Alternatively, we may speculate that the emergent symmetry could be exact. In this scenario, the dominant symmetry breaking field is tuned to zero at the first-order AFM-PSS transition and higher-order O(4) violating perturbations are either absent or vanish upon renormalization, by some extension of the DQCP description of the order parameters or by some more general mechanism. While emergent O(N) symmetric multicritical points arising from

$O(N - 1)$ and Z_2 order parameters have been extensively discussed within the LGW framework [43–45], the influence of the higher symmetry on associated first-order lines have not been addressed until recently in the DQCP context [25].

It would also be good to test whether the putative DQCP transition studied in Ref. [27] between similar states could actually be of the kind discussed here. Likewise, the previously argued $O(3)$ superfluid to charge-density-wave quantum critical point in a 2D hard-core boson system [46] might also be a weak first-order transition with enhanced symmetry.

The CBJQ model was designed with the quasi-2D material $\text{SrCu}_2(\text{BO}_3)_2$ in mind. In future experiments, the expected Ising-type $T > 0$ paramagnetic–PSS transition would be a good target for detecting emergent $O(4)$ symmetry. In 2D we expect $T_c \rightarrow 0$ continuously (logarithmically) [40, 47] as the $T = 0$ transition point is approached versus pressure, but 3D effects should push the first-order transition to $T > 0$, above which remnant $O(4)$ fluctuations may be observable.

Acknowledgments.—We would like to thank Fakher Asaad, Ribhu Kaul, Naoki Kawashima, Shiliang Li, Zi Yang Meng, Adam Nahum, Ying Ran, Subir Sachdev, Hui Shao, Liling Sun, and Zhi-Cheng Yang for stimulating discussions. This work was supported by the NSF under Grant No. DMR-1710170 and by a Simons Investigator Award. The calculations were carried out on Boston University’s Shared Computing Cluster.

* sandvik@bu.edu

- [1] S. Sachdev, Quantum magnetism and criticality, *Nature Phys.* **4**, 173 (2008).
- [2] R. K. Kaul, R. G. Melko, and A. W. Sandvik, Bridging Lattice-Scale Physics and Continuum Field Theory with Quantum Monte Carlo Simulations, *Annu. Rev. Condens. Matter Phys.* **4**, 179 (2013).
- [3] T. Senthil, A. Vishwanath, L. Balents, S. Sachdev, and M. P. A. Fisher, Deconfined Quantum Critical Points, *Science* **303**, 1490 (2004).
- [4] T. Senthil, L. Balents, S. Sachdev, A. Vishwanath, and M. P. A. Fisher, Quantum criticality beyond the Landau-Ginzburg-Wilson paradigm, *Phys. Rev. B* **70**, 144407 (2004).
- [5] A. W. Sandvik, Evidence for Deconfined Quantum Criticality in a Two-Dimensional Heisenberg Model with Four-Spin Interactions, *Phys. Rev. Lett.* **98**, 227202 (2007).
- [6] R. G. Melko and R. K. Kaul, Scaling in the Fan of an Unconventional Quantum Critical Point, *Phys. Rev. Lett.* **100**, 017203 (2008).
- [7] F.-J. Jiang, M. Nyfeler, S. Chandrasekharan, and U.-J. Wiese, From an antiferromagnet to a valence bond solid: evidence for a first-order phase transition, *J. Stat. Mech.* (2008) P02009.
- [8] A. B. Kuklov, M. Matsumoto, N. V. Prokofev, B. V. Svistunov, and M. Troyer, Deconfined Criticality: Generic First-Order Transition in the $SU(2)$ Symmetry Case, *Phys. Rev. Lett.* **101**, 050405 (2008).
- [9] J. Lou, A. W. Sandvik, and N. Kawashima, Antiferromagnetic to valence-bond-solid transitions in two-dimensional $SU(N)$ Heisenberg models with multispin interactions, *Phys. Rev. B* **80**, 180414(R) (2009).
- [10] A. W. Sandvik, Continuous Quantum Phase Transition between an Antiferromagnet and a Valence-Bond Solid in Two Dimensions: Evidence for Logarithmic Corrections to Scaling, *Phys. Rev. Lett.* **104**, 177201 (2010).
- [11] K. Chen, Y. Huang, Y. Deng, A. B. Kuklov, N. V. Prokofev, and B. V. Svistunov, Deconfined Criticality Flow in the Heisenberg Model with Ring-Exchange Interactions, *Phys. Rev. Lett.* **110**, 185701 (2013).
- [12] K. Harada, T. Suzuki, T. Okubo, H. Matsuo, J. Lou, H. Watanabe, S. Todo, and N. Kawashima, Possibility of deconfined criticality in $SU(N)$ Heisenberg models at small N , *Phys. Rev. B* **88**, 220408(R) (2013).
- [13] M. S. Block, R. G. Melko, and R. K. Kaul, Fate of CP^{N-1} Fixed Points with q Monopoles, *Phys. Rev. Lett.* **111**, 137202 (2013).
- [14] S. Pujari, K. Damle, and F. Alet, Néel-State to Valence-Bond-Solid Transition on the Honeycomb Lattice: Evidence for Deconfined Criticality, *Phys. Rev. Lett.* **111**, 087203 (2013).
- [15] A. Nahum, J.T. Chalker, P. Serna, M. Ortuño, and A.M. Somoza, Deconfined Quantum Criticality, Scaling Violations, and Classical Loop Models, *Phys. Rev. X* **5**, 041048 (2015).
- [16] H. Shao, W. Guo, and A. W. Sandvik, Quantum criticality with two length scales, *Science* **352**, 213 (2016).
- [17] M. Zayed, Ch. Rüegg, J. Larrea, A. M. Läuchli, C. Panagopoulos, S. S. Saxena, M. Ellerby, D. McMorr, Th. Strässle, S. S. Klotz, G. Hamel, R. A. Sadykov, V. Pomjakushin, M. Boehm, M. Jiménez-Ruiz, A. Schneidewin, E. Pomjakushin, M. Stingaciu, K. Conder, and H. M. Rønnow, 4-spin plaquette singlet state in the Shastry-Sutherland compound $\text{SrCu}_2(\text{BO}_3)_2$, *Nat. Phys.* **13**, 962 (2017).
- [18] B. S. Shastry and B. Sutherland, Exact ground state of a quantum mechanical antiferromagnet, *Physica B+C* **108**, 1069 (1981).
- [19] P. Corboz and F. Mila, Tensor network study of the Shastry-Sutherland model in zero magnetic field, *Phys. Rev. B* **87**, 115144 (2013).
- [20] A. Nahum, P. Serna, J. T. Chalker, M. Ortuño, and A. M. Somoza, Emergent $SO(5)$ Symmetry at the Néel to Valence-Bond-Solid Transition, *Phys. Rev. Lett.* **115**, 267203 (2015).
- [21] A. Karch and D. Tong, Particle-Vortex Duality from 3D Bosonization, *Phys. Rev. X* **6**, 031043 (2016).
- [22] M. A. Metlitski and A. Vishwanath, Particle-Vortex Duality of Two-Dimensional Dirac Fermion from Electric-Magnetic Duality of Three-Dimensional Topological Insulators, *Phys. Rev. B* **93**, 245151 (2016).
- [23] D. F. Mross, J. Alicea, and O. I. Motrunich, Explicit Derivation of Duality between a Free Dirac Cone and Quantum Electrodynamics in $(2+1)$ Dimensions, *Phys. Rev. Lett.* **117**, 016802 (2016).
- [24] S. Kachru, M. Mulligan, G. Torroba, and H. Wang, Non-supersymmetric Dualities from Mirror Symmetry, *Phys. Rev. Lett.* **118**, 011602 (2017).
- [25] C. Wang, A. Nahum, M. A. Metlitski, C. Xu, and T. Senthil, Deconfined Quantum Critical Points: Symmetries and Dualities, *Phys. Rev. X* **7**, 031051 (2017).
- [26] Y. Q. Qin, Y.-Y. He, Y.-Z. You, Z.-Y. Lu, A. Sen, A. W. Sandvik, C. Xu, and Z. Y. Meng, Duality between the Deconfined Quantum-Critical Point and the Bosonic Topological Transition, *Phys. Rev. X* **7**, 031052 (2017).
- [27] T. Sato, M. Hohenadler, and F. F. Assaad, Dirac Fermions with Competing Orders: Non-Landau Transition with Emergent Symmetry, *Phys. Rev. Lett.* **119**, 197203 (2017).
- [28] M. A. Metlitski and R. Thorngren, Intrinsic and emergent anomalies at deconfined critical points, arXiv:1707.07686.

- [29] S. Gazit, F. F. Assaad, S. Sachdev, A. Vishwanath, and C. Wang, Confinement transition of Z_2 gauge theories coupled to massless fermions: emergent QCD3 and $SO(5)$ symmetry, arXiv:1804.01095.
- [30] G. J. Sreejith, S. Powell, and A. Nahum, Emergent $SO(5)$ symmetry at the columnar ordering transition in the classical cubic dimer model, arXiv:1803.11218.
- [31] A. W. Sandvik and H. G. Evertz, Loop updates for variational and projector quantum Monte Carlo simulations in the valence-bond basis, Phys. Rev. B **82**, 024407 (2010).
- [32] A. W. Sandvik, Computational Studies of Quantum Spin Systems, AIP Conf. Proc. **1297**, 135 (2010).
- [33] A. W. Sandvik, Finite-size scaling and boundary effects in two-dimensional valence-bond solids, Phys. Rev. B **85**, 134407 (2012).
- [34] T. Senthil and M. P. A. Fisher, Competing orders, nonlinear sigma models, and topological terms in quantum magnets, Phys. Rev. B **74**, 064405 (2006).
- [35] Our calculations cannot distinguish between $O(4)$ and $SO(4)$ symmetry, since we only test for the rotational symmetry common to both.
- [36] J. M. Luck, Corrections to finite-size-scaling laws and convergence of transfer-matrix methods, Phys. Rev. B **31**, 3069 (1985).
- [37] K. Vollmayr, J. D. Reger, M. Scheucher, and K. Binder, Finite size effects at thermally-driven first order phase transitions: A phenomenological theory of the order parameter distribution, Z. Phys. B **91**, 113 (1993).
- [38] S. Iino, S. Morita, A. W. Sandvik, and N. Kawashima, Detecting signals of weakly first-order phase transitions in two-dimensional Potts models, arXiv:1801.02786.
- [39] A. Sen and A. W. Sandvik, Example of a first-order Néel to valence-bond-solid transition in two dimension, Phys. Rev. B **82**, 174428 (2010).
- [40] A. Cuccoli, T. Roscilde, V. Tognetti, R. Vaia, and P. Verrucchi, Quantum Monte Carlo study of $S = 1/2$ weakly anisotropic antiferromagnets on the square lattice, Phys. Rev. B **67**, 104414 (2003).
- [41] M. E. Muller, A note on a method for generating points uniformly on n-dimensional spheres, Commun. ACM **2**(4), 19 (1959).
- [42] See Supplemental Material for detailed definitions and quantitative analysis of the $O(4)$ symmetry.
- [43] A. Pelissettp and E. Vicari, Multicritical behavior of two-dimensional anisotropic antiferromagnets in a magnetic field, Phys. Rev. B **76**, 024436 (2007).
- [44] M. Hasenbusch and E. Vicari, Anisotropic perturbations in three-dimensional $O(N)$ -symmetric vector models, Phys. Rev. B **84**, 125136 (2011).
- [45] A. Eichorn, D. Mesterházy, and M. M. Scherer, Multicritical behavior in models with two competing order parameters, Phys. Rev. B **88**, 042141 (2013).
- [46] F. Hébert, G. G. Batrouni, R. T. Scalettar, G. Schmid, M. Troyer, and A. Dorneich, Quantum phase transitions in the two-dimensional hardcore boson model, Phys. Rev. B **65**, 014513 (2001).
- [47] V. Yu. Irkhin and A. A. Katanin, Thermodynamics of isotropic and anisotropic layered magnets: Renormalization-group approach and $1/N$ expansion, Phys. Rev. B **57**, 379 (1998).
- [48] S. Liang, B. Doucot, and P. W. Anderson, Some New Variational Resonating-Valence-Bond-Type Wave Functions for the Spin-1/2 Antiferromagnetic Heisenberg Model on a Square Lattice, Phys. Rev. Lett. **61**, 365 (1988).
- [49] K. S. D. Beach and A. W. Sandvik, Some formal results for the valence bond basis, Nucl. Phys. B **750**, 142 (2006).
- [50] A. W. Sandvik, Stochastic series expansion method with operator-loop update, Phys. Rev. B **59**, R14157 (1999).
- [51] H. G. Evertz, The Loop Algorithm, Adv. Phys. **52**, 1 (2003).
- [52] U. Wolff, Collective Monte Carlo Updating for Spin Systems, Phys. Rev. Lett. **62**, 361 (1989).

SUPPLEMENTAL MATERIAL

Symmetry enhanced first-order phase transition in a two-dimensional quantum magnet

B. Zhao, P. Weinberg, and A. W. Sandvik

Here we discuss further details of our tests of emergent $O(4)$ symmetry based on order-parameter distributions (histograms) $P(m_z, m_p)$ such as those shown in Fig. 5. In addition, we also consider the distribution of $P(m_s, m_p)$, where m_s is the full $O(3)$ AFM order parameter,

$$m_s^2 = m_x^2 + m_y^2 + m_z^2, \quad (\text{S1})$$

which, like m_p defined in Eqs. (3) and (7), is obtained in the valence-bond projector QMC method after each Monte Carlo updating sweep directly from the transition graph as a single unique number (in contrast to just the component m_z , which is obtained by sampling one of the many spin configurations that contribute to the transition graph). Note that it is not possible to obtain independent equal-time values for all three components of the AFM order parameter from the transition graphs or the associated z basis spin configurations.

In the simulations, we generate and store a long list of points $(m_z, m_s^2, m_p)_i$, $i = 1, \dots, N$. In order to obtain smooth probability distributions and small error bars on the associated integrated quantities that we use to test for the emergent symmetry, we need a very large number of points (N of the order of millions) and this currently limits the accessible system size to $L = 64$.

Symmetry tests with two components.—The definitions of the two order parameters by Eqs. (3) and (7) are not unique, and, therefore, even if there is an emergent symmetry between the order parameters, m_z and m_p are not directly comparable as to their overall magnitudes. To investigate a possible emergent $O(2)$ symmetry of the distribution $P(m_z, m_p)$, as a proxy for the full $O(4)$ symmetry of all four components, we need to remove the ambiguity by properly normalizing the sampled numbers. To this end, post-simulation, we compute the corresponding variances $\langle m_z^2 \rangle$ and $\langle m_p^2 \rangle$. We can then define the radius R of the distribution as

$$\langle R^2 \rangle = \langle m_z^2 \rangle + a^2 \langle m_p^2 \rangle, \quad R \equiv \langle R^2 \rangle^{1/2}, \quad (\text{S2})$$

while also requiring that

$$\langle m_z^2 \rangle = a^2 \langle m_p^2 \rangle. \quad (\text{S3})$$

Thus, the parameter a that puts the two sampled order parameters on an equal scale is defined by

$$a^2 = \frac{\langle m_z^2 \rangle}{\langle m_p^2 \rangle}. \quad (\text{S4})$$

We can now define normalized point pairs as

$$(\tilde{m}_z, \tilde{m}_p) = R^{-1}(m_z, am_p), \quad (\text{S5})$$

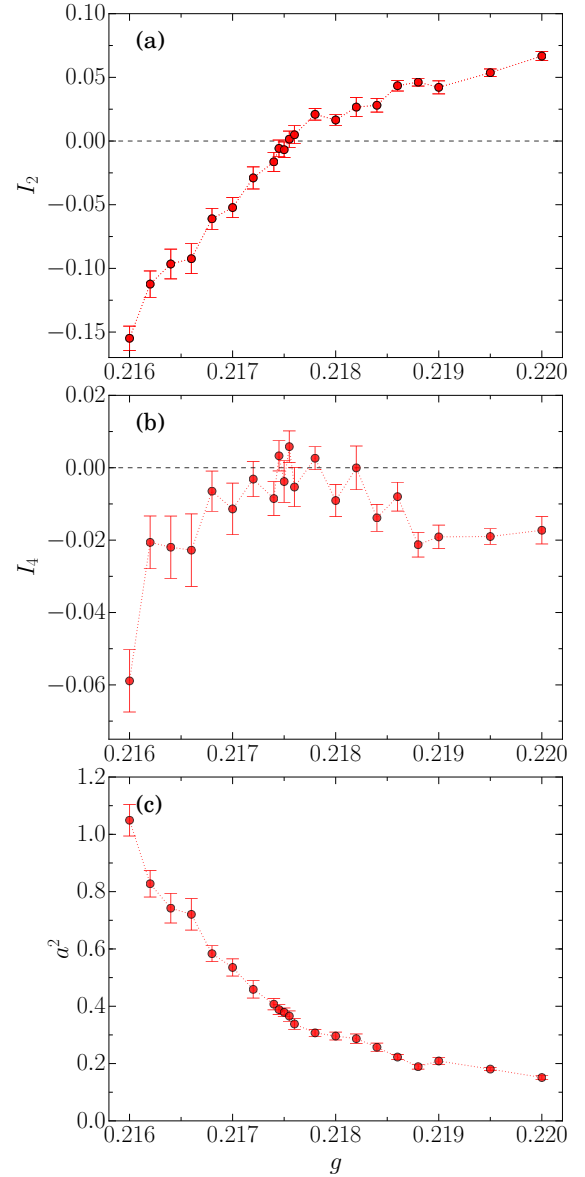


Figure S1. Tests of emergent $O(4)$ symmetry in the CBJQ model using the integrals I_n in Eq. (S6), with $n = 2$ and 4 . The results are shown versus the coupling ratio in panels (a) and (b), and in (c) the parameter a^2 , Eq. (S4), required to equalize the arbitrary lengths of the AFM and PSS vector components is shown on the same scale.

and test for emergent $O(2)$ symmetry in the distribution $P(\tilde{m}_z, \tilde{m}_p)$ at the AFM-PSS transition.

There is still a remaining ambiguity here, as to the point at which the scale factor a should be evaluated. In Fig. 5(a) of the main paper, a was evaluated at $g = 0.21745$ (the data in the middle panel) and used at the other g values as well. If the distribution is $O(2)$ symmetric at g_c , as it appears to be, it is indeed most natural to fix a at this point, instead of using a g -dependent value $a(g)$ computed from a distribution that is not $O(2)$ symmetric when $g \neq g_c$. However, to test the emergent symmetry more systematically and to find the point, for given L , at which the symmetry is the highest, we have to follow a

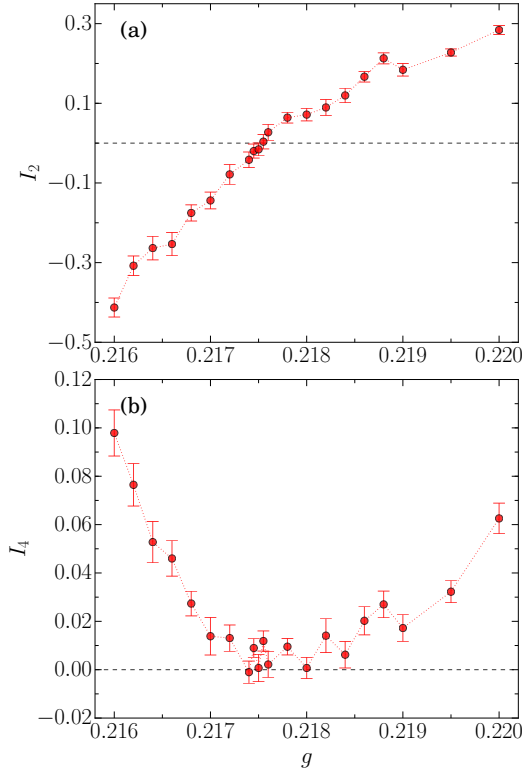


Figure S2. Alternative tests of emergent O(4) symmetry, using the integrals I_2 (a) and I_4 (b) where the value of the length re-scaling parameter a in Eq. (S4) is held fixed at the value obtained in Fig. S1(c) at the point $g = 0.21745$ where I_2 crosses 0.

two-step procedure that we describe next.

To quantify the degree of O(2) symmetry of a distribution $P(\tilde{m}_z, \tilde{m}_p)$ we use the integrals

$$\begin{aligned}
 I_q &= \int d\tilde{m}_z d\tilde{m}_p P(\tilde{m}_z, \tilde{m}_p) \cos(q\phi(\tilde{m}_z, \tilde{m}_p)) \\
 &= \frac{1}{N} \sum_{i=1}^N \cos(q\phi(|\tilde{m}_z|, |\tilde{m}_p|)_i), \quad (\text{S6})
 \end{aligned}$$

where on the second line i is the index corresponding to the N QMC sampled points $(m_z, m_p)_i$, from which angles $\phi(|\tilde{m}_z|, |\tilde{m}_p|)_i \in [0, \pi/2]$ are extracted (with the absolute values taken to transform to the positive quadrant). We will here consider the integrals I_2 and I_4 , both of which should vanish if the distribution is O(2) symmetric. For larger n the results become increasingly noisy, but since there is no reason to expect distributions with $I_2 = I_4 = 0$ and $I_{n>4} \neq 0$, what we do is enough for demonstrating O(4) symmetry.

At the first stage, we compute the scale factor $a = a(g)$ in Eq. (S4) for each of the g values considered and use these values when evaluating I_2 and I_4 based on the rescaled point pairs in Eq. (S5). Results for the $L = 64$ CBJQ model are shown in Figs. S1(a,b), and the scale factor $a^2(g)$ is shown in Fig. S1(c). We can see that I_2 crosses 0 very close to the g value for which data are shown in the middle panel of Fig. 5, and this value is also very close to the transition point g_c . We

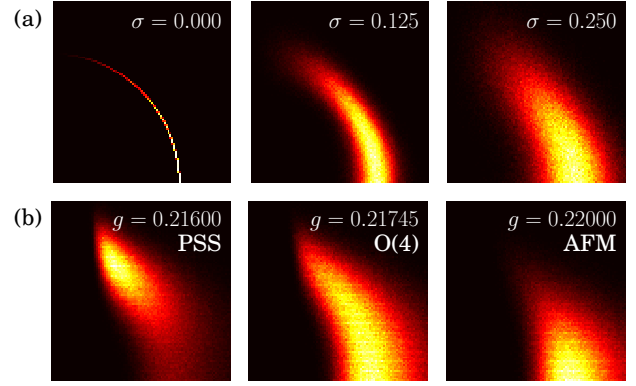


Figure S3. Test of emergent O(4) symmetry of the CBJQ involving all four order parameter components. The x axis represents the magnitude of the total AFM order parameter m_s , defined in Eq. (S1), and the vertical axis the PSS order parameter m_p . Only the quadrant with all positive values is shown. Panels (a) are for the case of a perfect O(4) sphere with radius $R = 1$ and variance σ^2 , sampled using the algorithm in Ref. [41]. Panels (b) show valence-bond projector QMC results for the CBJQ model at three values of g ; inside the PSS phase, close to the transition point with emergent O(4) symmetry, and inside the AFM phase.

can also see that I_4 is statistically indistinguishable from 0 in the neighborhood of the same point, while further away from g_c the values are clearly negative. These results confirm that there is a point at which we can not detect any deviations from O(2) symmetry to within the error bars.

The g -dependent value of a used above is not ideal, in the sense that it tends to bring the rescaled distribution as close as possible to O(2) symmetry even when there is no O(2) symmetry, by enforcing the condition Eq. (S3) that should not necessarily be obeyed away from the O(2) point. We therefore also recompute I_2 and I_4 with a fixed at its value where the previously computed I_2 crosses 0, i.e., from the data in Figs. S1(a,c). The results are shown in Fig. S2. Here we can see larger variations in I_2 and I_4 versus g , and I_4 now exhibits a much more clearly defined point, a minimum, at which the symmetry is obeyed most closely. The minimum value equals 0 to within statistical errors and it is located at the g value where I_2 crosses 0, again fully supporting the emergent O(2) symmetry. We also see this behavior for $L = 32$ (not shown) but with a much wider minimum. With increasing size, we indeed expect the distribution to narrow as a power of $1/L$, but, because of the long simulation run times required to obtain smooth distributions, we have so far not gone higher than $L = 64$ with these tests.

The O(4) symmetry projected down to two components also implies a flat radial distribution between 0 and the radius R of the sphere. As we pointed out in the main text and demonstrated in Fig. 5, the not completely flat behavior close to the rim observed in the CBJQ histogram can be explained by fluctuations of the radius, which should vanish only in the limit $L \rightarrow \infty$. Furthermore, since the O(3) symmetry between the three components of the AFM order parameter is explic-

itly enforced by the Hamiltonian and also not violated in any way in the simulations, the demonstration of O(2) symmetry in the distribution $P(m_z, m_p)$ immediately also implies O(4) symmetry at the AFM-PSS coexistence point. Thus, we have shown here that the $L = 64$ CBJQ model has a point at which its combined AFM and PSS order parameters exhibit O(4) symmetry to a high degree, with violations that are too small to be detectable within the rather small error bars.

Tests with four components.—We complement the above analysis of two out of the four components of the putative O(4) vector with a test where all four components are used, projected down to two dimensions by using the magnitude of the full O(3) AFM order parameter in Eq. (S1) and the PSS order parameter, i.e., the distribution $P(m_s, m_p)$. We carry out a process similar to the one discussed above to put the overall lengths of the AFM and PSS components on equal footing.

For an ideal O(4) sphere with fixed R projected down to two dimensions in this manner, the distribution $P(m_s, m_p)$ has the shape of arc of infinitesimal thickness and radius R , with the density varying proportionally to m_s^2 along the arc, due to the different contents of the two dimensions. Fig. S3(a) shows the distribution for three different values of the standard deviation σ of the fluctuating radius about the mean value $R = 1$. In the case of the CBJQ model, as shown in Fig. S3(b), there is

indeed very little weight close to the y-axis as expected. As we go from the PSS state to the AFM state the weight shifts clockwise from large y (m_p) values down toward the x -axis (large m_s). At the transition point we see a distribution very similar to the O(4) sphere with $\sigma \approx 0.25$

It should be noted that m_s^2 in the valence bond basis is obtained from the transition graph as a sum of squared loop lengths, and this corresponds to a sum over 2^{n_l} spin configurations in the basis of S^z spins, n_l being the number of loops (each loop having two compatible staggered spin configurations). This implicit averaging over points on the putative O(4) sphere may cause some additional smearing in $P(m_s, m_p)$, beyond just the projection down to two dimensions and the fluctuations of the radius associated with finite system size. The larger σ required to match the O(4) sphere in Fig. S3 than what was needed in the case of $P(m_z, m_p)$ in Fig. 5 likely reflects this effect. In addition, for finite system size, the loop estimator for m_s has a strict lower bound $\propto 1/N$, with a de facto large prefactor, and this also seems to cause some visible deviations from the O(4) sphere results at the left tip of the distribution. For these reasons, we believe that the $P(m_z, m_p)$ distribution is better for quantitatively characterizing the degree of symmetry.